Experimental investigation on cyclic in-plane behavior of URM walls retrofitted with AFRP

Zamani-Ahari, Gholamreza
Department of Civil Engineering, Faculty of Engineering, Urmia University

Yamaguchi, Kentaro
Department of Architecture and Urban Design, Faculty of Human-Environment Studies, Kyushu University

出版情報：Case Studies in Construction Materials. 17, pp.e01558-, 2022-12. Elsevier
バージョン：

Case Studies in Construction Materials 17 (2022) e01558

Contents lists available at ScienceDirect

Case Studies in Construction Materials

journal homepage: www.elsevier.com/locate/cscm

Experimental investigation on cyclic in-plane behavior of URM walls retrofitted with AFRP

Gholamreza Zamani-Ahari [a,*], Kentaro Yamaguchi [b]

[a] Department of Civil Engineering, Faculty of Engineering, Urmia University, Urmia, Iran
[b] Department of Architecture and Urban Design, Faculty of Human-Environment Studies, Kyushu University, Fukuoka, Japan

ARTICLE INFO

Keywords:
AFRP
Cyclic behavior
Shear strength
Seismic retrofitting
Unreinforced masonry wall

ABSTRACT

URM buildings have been the most common constructions globally, although they are weak because of their low lateral strength against seismic loads. The seismic response of URM structures is highly dependent on the in-plane and out-of-plane behaviors of their load-carrying walls. As in-plane behavior, the shear failure has been known as the most brittle failure mode of URM walls. Although the monotonic response of the walls has been investigated widely, there is relatively less knowledge about their hysteretic response as well as the impact of seismic retrofitting on it. Considering the brittle nature of the in-plane behavior, the Aramid Fiber Reinforced Polymer (AFRP) sheet as a relatively soft member of FRP products was chosen as the retrofitting choice in this study. As an experimental study, cyclic lateral loading was applied to the bare and AFRP retrofitted masonry wall specimens in a displacement-controlled manner. To study the shear behavior of the AFRP retrofitted masonry wall specimens, the specimens were externally retrofitted with AFRP sheets in two different configurations; fully and diagonally wrapped. The load-deformation behavior of the walls during the cyclic loading was investigated using hysteresis diagrams. The test results revealed that AFRP retrofitting could improve the shear strength by about 75% and 81% for fully and diagonally wrapped specimens, respectively. Also, the integrity of URM walls was enhanced without altering their lateral stiffness. Moreover, the fully-wrapped specimen exhibited a deformation capability of about 37% higher than the diagonally-wrapped one. Furthermore, the failure of the fully-wrapped specimen was controlled by toe crushing of the masonry wall, while the rupture of the retrofitting sheet caused the failure in the diagonally-wrapped specimen.

1. Introduction

Unreinforced masonry structures have been one of the most common structures around the globe for a long time and, an estimated about seventy percent of worldwide structures are masonry [1]. There are several explanations for the popularity of this construction type, such as the convenience of constituents, constructional skills, familiarity with the masonry supplies, and lower building cost compared to other structure types [2]. There are plenty of these buildings in seismically active regions [3]. Masonry structures are prone to significant damage due to their weak seismic performance, which is mainly caused by the weak in-plane and out-of-plane responses of URM walls. URM walls play a crucial role in the initiation and propagation of damage during severe earthquakes due

* Corresponding author.
E-mail address: g.zamani@urmia.ac.ir (G. Zamani-Ahari).

https://doi.org/10.1016/j.cscm.2022.e01558
Received 14 May 2022; Received in revised form 27 September 2022; Accepted 10 October 2022
Available online 13 October 2022

to their substantially weak tensile behavior, high mass (high seismic inertia forces), low ductility, and stiffness softening after cracking which leads to partial or global collapse demonstrated as the in-plane or out-of-plane failure mechanisms of the load-bearing masonry walls [4,5].

The in-plane failure of the masonry walls includes bending sub-mode and shear sub-mode. The in-plane failure mode is demonstrated in four failure types, such as shear (diagonal), sliding, rocking, and crushing of toe, based on the amount of surcharge loading, the wall aspect ratio, boundary conditions of the wall, shear and compression strengths of masonry [6], [7]. Among the four mentioned failure types, the diagonal and sliding are associated with the shear behavior of the URM wall and occur due to two mechanisms. As the first mechanism - the most common in-plane failure mode of masonry walls due to seismic loads – the principal tensile stresses caused by the combination of lateral and vertical loads lead to cracking in the diagonal direction of the wall. The initiation of the cracks depends on the mortar to brick strength ratio so that they may occur in brick or mortar or the contact area of them. In the second mechanism, the brick rows slide because of the formation and propagation of a set of horizontal tensile micro-cracks. These micro-slides can potentially lead to the in-plane sliding of the wall at the horizontal joint of bricks. The rocking and crushing of toe failure types occur due to the large ratio of bending moment to shear force or high shear resistance of the masonry wall [8].

In order to enhance the seismic performance of unreinforced masonry structures, particular procedures are necessary to improve the lateral behavior of walls. Improving the seismic response of URM walls has been of interest to many researchers employing different retrofitting methods such as confining, pre-stressing, shotcrete, steel reinforcements, and epoxy injection. Most of these methods are time-consuming and costly and add considerable mass to the effective seismic mass of the structure. Besides, the corrosion of steel reinforcements is another drawback of these techniques [9]. Fiber reinforced cement as a relatively new construction mortar exhibited considerable strength and ductility [10]. Due to the negligible increase in effective seismic weight, easy installation, cost-effectiveness, and lower maintenance costs, fiber reinforced polymers (FRP) as relatively new materials have attracted more interest for application in masonry structures compared to the other retrofitting methods. Moreover, extensive recent research on their mechanical characteristics provided a proper understanding of their behavior for analysis and design [11]. The results of numerous studies showed that the application of FRPs such as carbon fiber reinforced polymer (CFRP), glass fiber reinforced polymer (GFRP) and basalt fiber reinforced polymer (BFRP) increases the lateral shear strength of the URM wall while it may decrease the ductility to the almost same extent [12–21].

Being a softer product in FRPs, aramid fiber reinforced polymer (AFRP) is regarded as an appropriate strengthening choice for masonry walls, which negligibly increases the wall stiffness. Zamani Ahari et al. [22] conducted a series of diagonal shear tests on small masonry specimens to grasp the effect of AFRP retrofitting. As a result, the AFRP sheet increased the shear strength of the masonry specimens and their ductility. Aramid fibers as reinforcement for advanced composites were developed in the 1960 s and introduced commercially by DuPont in the 1970 s under the trade name Kevlar. Kevlar fiber is five times stronger than steel exhibiting greater strength to weight ratio than carbon and glass fibers [23]. Brózda et al. [24] studied the simply supported concrete beams reinforced with aramid, carbon, and glass fiber reinforced composite bars under bending according to ACI 440.1 R-06 guidelines and investigated the difference in the results related to the specific properties of each fiber. The lowest value of the deflection was achieved in beams reinforced with AFRP bars. Also, a comprehensive investigation of the blast responses of AFRP-strengthened reinforced concrete slabs was reported by Kong et al. [25]. They found out that AFRP not only delays the concrete cracking but also changes the damage mode from localized spalling to FRP rupture and debonding.

While CFRP and GFRP have been widely studied for retrofitting masonry structures, AFRP has not been appropriately investigated in this regard. Besides, most research works concerning the in-plane behavior of the FRP retrofitted masonry walls have been conducted on a monotonic loading procedure which is different from its actual hysteretic behavior [26–30].

In the present study, cyclic loading was applied to the masonry walls in a displacement-controlled manner, and their failure mechanism, hysteretic behavior, and shear strength were investigated. The specimens were externally retrofitted with AFRP sheets in two different configurations; diagonally and fully wrapped. The obtained hysteresis diagrams of the retrofitted specimens were compared with the bare reference wall, and the obtained results were discussed thoroughly.

2. Experimental program

2.1. Materials

2.1.1. Aramid fiber reinforced polymer (AFRP)

Zhu et al. [31] studied the tensile stress versus strain curves in both warp and weft directions for AFRP woven sheets (also known as Kevlar 49 fabric). During the weaving process of the sheet, the warp remains stationary in the loom, while the weft weaves in and out as shown in Fig. 1. Aramid sheets are about one-fifth the weight of steel, so there is almost no increase in structural weight due to reinforcement. Aramid sheets do not rust, so there is no concern about re-deterioration in the future. Aramid sheets are flexible, so they can be easily applied to structural elements. Aramid sheet has good resin impregnation, so it has excellent construction reliability.

Since aramid sheets do not conduct electricity, there is no risk of electrical corrosion of reinforcing bars in RC elements. Aramid sheet does not deteriorate or rust due to moisture. Moreover, aramid sheets are extremely resistant to impact loading[i]. Results indicated that the elastic stiffness (Young's modulus) of the warp direction is almost identical to the one of the weft direction. The

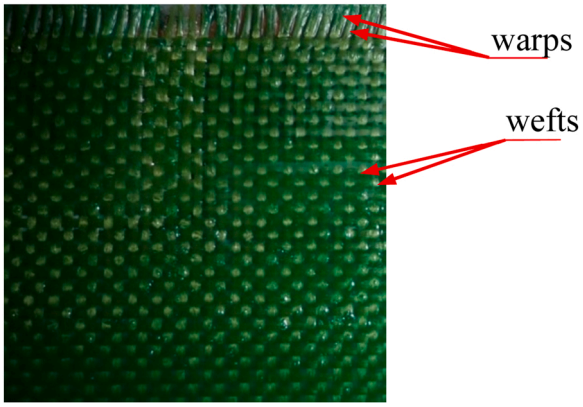

Fig. 1. AFRP fabric.

Table 1
Properties of AFRP sheet (Kevlar 49 fabric) [22].[a]

Product typ	*Weight (g/cm^3)*	*Tensile capacity (kN/m)*	*Thickness (mm)*	*Tensile strength (N/mm^2)*	*Young's modulus (kN/mm^2)*
AK- 10/10	*180*	*98/98*	*0.048*	*2060*	*118*

[a] FIBEX Co. Ltd. http://www.fibex.co.jp.

properties of the AFRP sheet product obtained from the company that provided the AFRP sheets for this study are presented in Table 1 [22]. An acrylic adhesive was used for adhering the retrofit sheet to the masonry substrate which is a resin-based, two-part adhesive comprised of acrylic or methyl acrylic polymers. This type of adhesive is inherently stable to UV light and oxidation, resistant to chemicals, and is generally preferred for outdoor applications.[1] The retrofitting process as shown schematically in Fig. 2 started with polishing the masonry surface. Then putty was applied to the specimen to provide a plain substrate. Finally, the resin adhesive was applied and a ruler was employed to ensure a full bond between the substrate and sheet.

2.1.2. Masonry brick

The experimental specimens were built using fired clay bricks with dimensions of 210 × 110 × 60 (length× width× height) mm. The brick and mortar test setups are demonstrated in Fig. 3. From the results of an earlier investigation conducted by the authors, the mechanical properties of the bricks, such as compressive strength, flexural strength, and elastic modulus following ASTM C67 [32] were obtained as 9 MPa, 64.5 MPa, and 17.7 GPa, respectively [33]. Also, the compressive test on prism was conducted following ASTM C1314 [34] from previous research that demonstrated the compressive strength of masonry as 30.1 MPa [33].

2.1.3. Joint mortar

A mixture of Portland cement (1), sand (6.5), and silica powder (1) was used in mixing the mortar, and the W/C (water-to-cement) ratio was taken as 130%. The mechanical properties of the joint mortar and followed standards are indicated in Table 2 (results of an earlier investigation conducted by the authors) [33].

2.2. Masonry specimens

Three masonry brick walls were built with dimensions of 110 (thickness) × 1060 (height) × 1090 (length) mm. The joint mortar thickness was 10 mm. The aspect ratio of the walls was adopted at approximately equal to 1 to impose a shear failure mode.

The specimens were constructed on top of the reinforced concrete beams with dimensions of 2050 (width) × 300 (height) × 350 (length) mm. Once the specimens had been cured, another reinforced concrete beam with dimensions of 2050 (width) × 400 (height) × 350 (length) mm was mounted on top of each specimen. A hydraulic jack attached to the upper beam was employed to apply the cyclic loading. To prevent slipping in the beam-wall interface, steel angles were attached to the top and bottom beams.

2.3. Retrofitting

The wall specimens were retrofitted in two configurations; diagonally and fully wrapped. As the fully-wrapped pattern (AFRP-F), the AFRP sheets with dimensions of 1090 × 1060 mm were adhered to both sides of the wall using epoxy, as shown in Fig. 4(a). In the diagonally-wrapped pattern (AFRP-X), the AFRP sheets with dimensions of 250 × 1520.4 mm were adhered, as shown in Fig. 4(b).

[1] FIBEX Co. Ltd. http://www.fibex.co.jp.

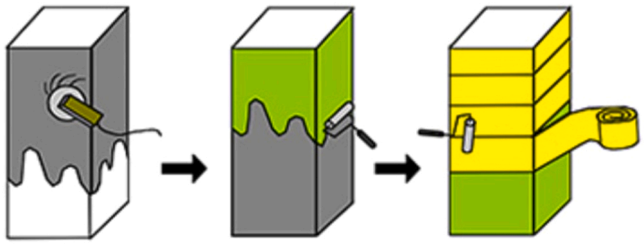

Fig. 2. Retrofitting process.

Fig. 3. Brick and mortar tests.

Table 2
Properties of joint mortar [33].

Property	
Flow (mm) (ASTM C1437) [35]	*157*
Unit weight (g/cm^3) (ASTM C138) [36]	*1.96*
Elastic modulus (GPa) (ASTM C469) [37]	*12.30*
Poisson's ratio (ASTM C469) [37]	*0.16*
Compressive strength (MPa) (ASTM C109) [38]	*10*

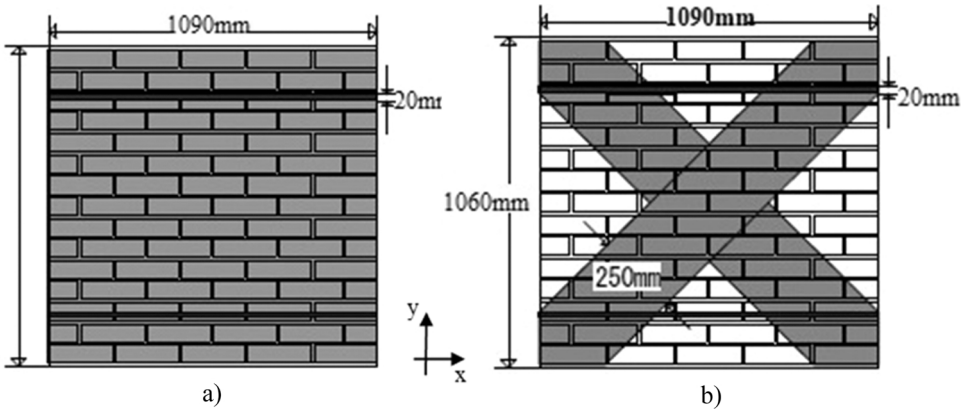

Fig. 4. AFRP retrofitted specimens, a) AFRP-F b) AFRP-X.

Furthermore, to avoid immature detachment (debonding) of AFRP sheets from the wall surface, AFRP bands with a thickness of 20 mm were utilized to reach the maximum capacity of the retrofitted wall specimen. Pictures of the retrofitted walls with both retrofitting patterns and the LVTDs mounting setup are shown in Fig. 5.

2.4. Cyclic test setup

The test setup, measuring tools, loading apparatus, and details of connections are illustrated in Figs. 6–9. The cyclic test setup consists of the rigid floor, reaction frame, actuator, and load cells. The lateral and vertical loads – representing seismic and gravity loads - were applied to the walls. The lateral loading generated by the hydraulic jack caused the wall specimen to move horizontally. The loading system is shown in Fig. 9. To ensure the occurrence of shear failure, the lateral loading was controlled by four load cells connected to the top beam. Furthermore, the out-of-plane behavior of the specimens was prevented using a lateral support system

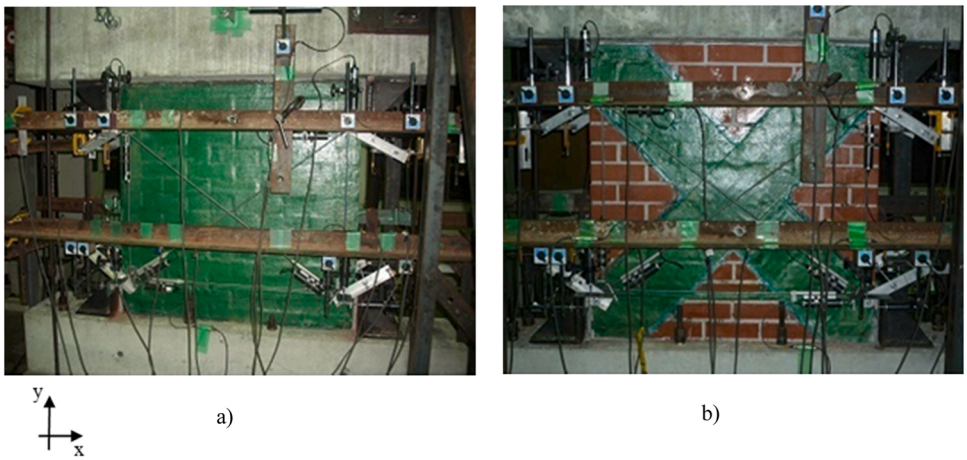

Fig. 5. Pictures of AFRP retrofitted specimens, a) AFRP-F b) AFRP-X.

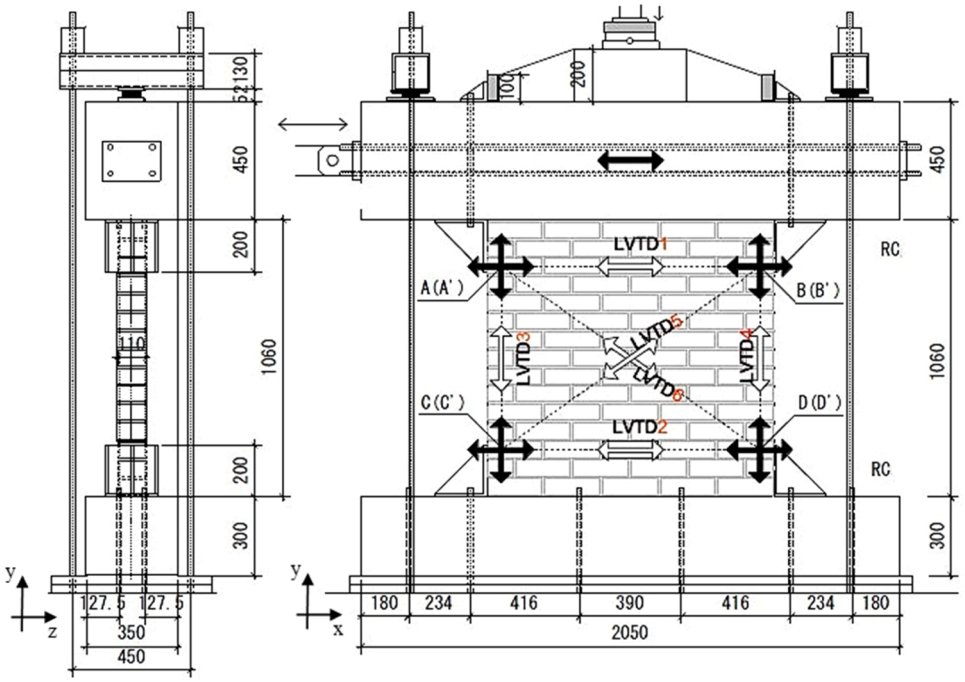

Fig. 6. Dimensions of specimens and test setup.

shown in Fig. 9, and the specimens could only move in a horizontal direction under applied loading.

To prevent unwanted movements, the lower beam was firmly fastened to the rigid floor using bolts. Twelve displacement meter devices (LVDT) were utilized to measure displacements as illustrated in Fig. 6. Two devices (LVDT1, 2) displayed in Fig. 6 were used for measuring horizontal displacements, another two (LVDT3, 4) for vertical displacements, and two (LVDT5, 6) for diagonal displacement at each side of the wall. The LVDT 1 and its other side counterparts were attached to the specimen in the middle of the third row of brick (from the bottom). The exact vertical distance between LVDT1 and LVDT2 was 700 mm. The lateral deformation angle (%rad) was calculated by dividing the relative horizontal displacement of the specimen – the difference between average recorded data by LVDT1 and its other side counterpart and the average recorded data by LVDT2 and its other side counterpart – by 700 mm.

2.5. Loading pattern

A vertical load of 0.35 MPa was applied to the top beam. The displacement-controlled lateral loading protocol suggested by FEMA 461 [39] was employed. The protocol is demonstrated in Fig. 10. In this loading protocol, each deformation angle was applied to the

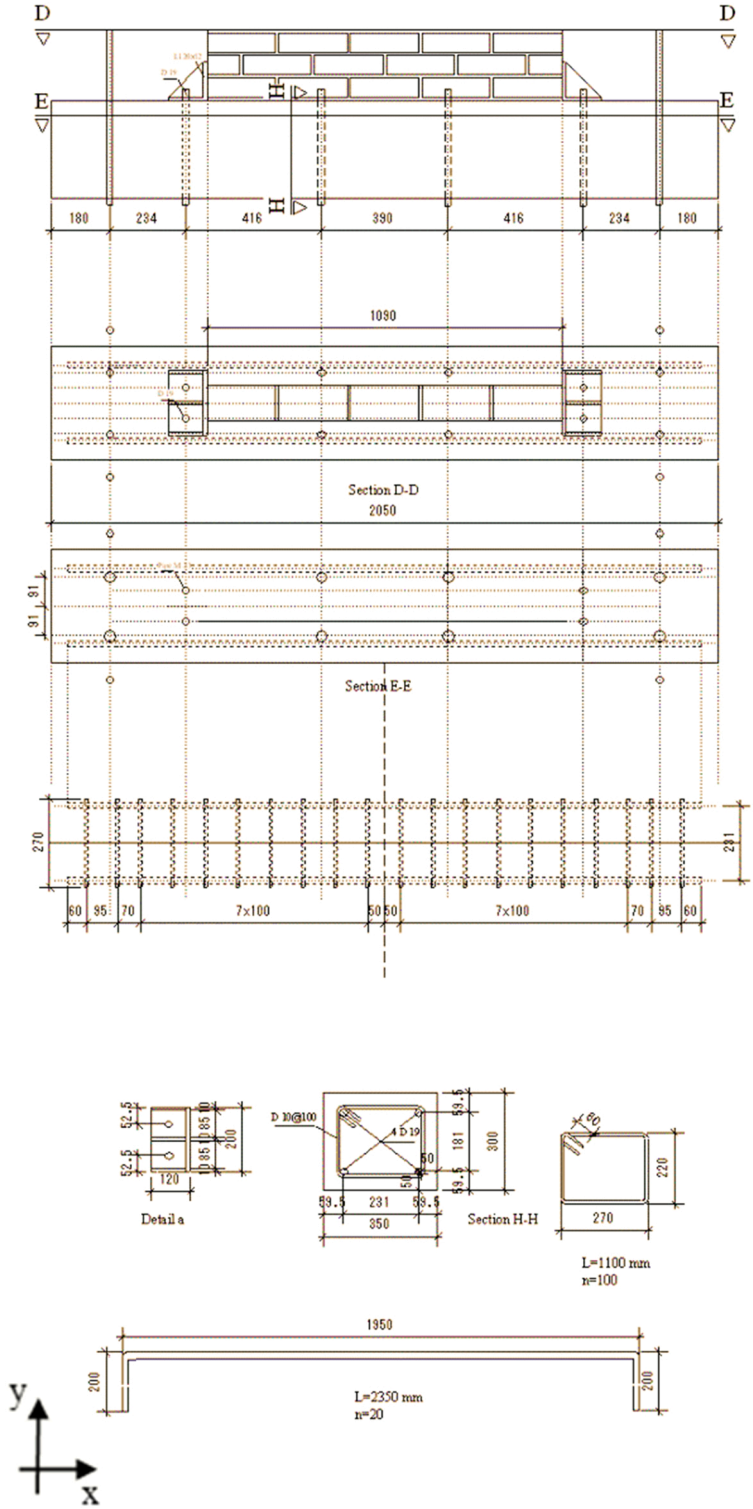

Fig. 7. Detailes of connection of specimen to bottom beam.

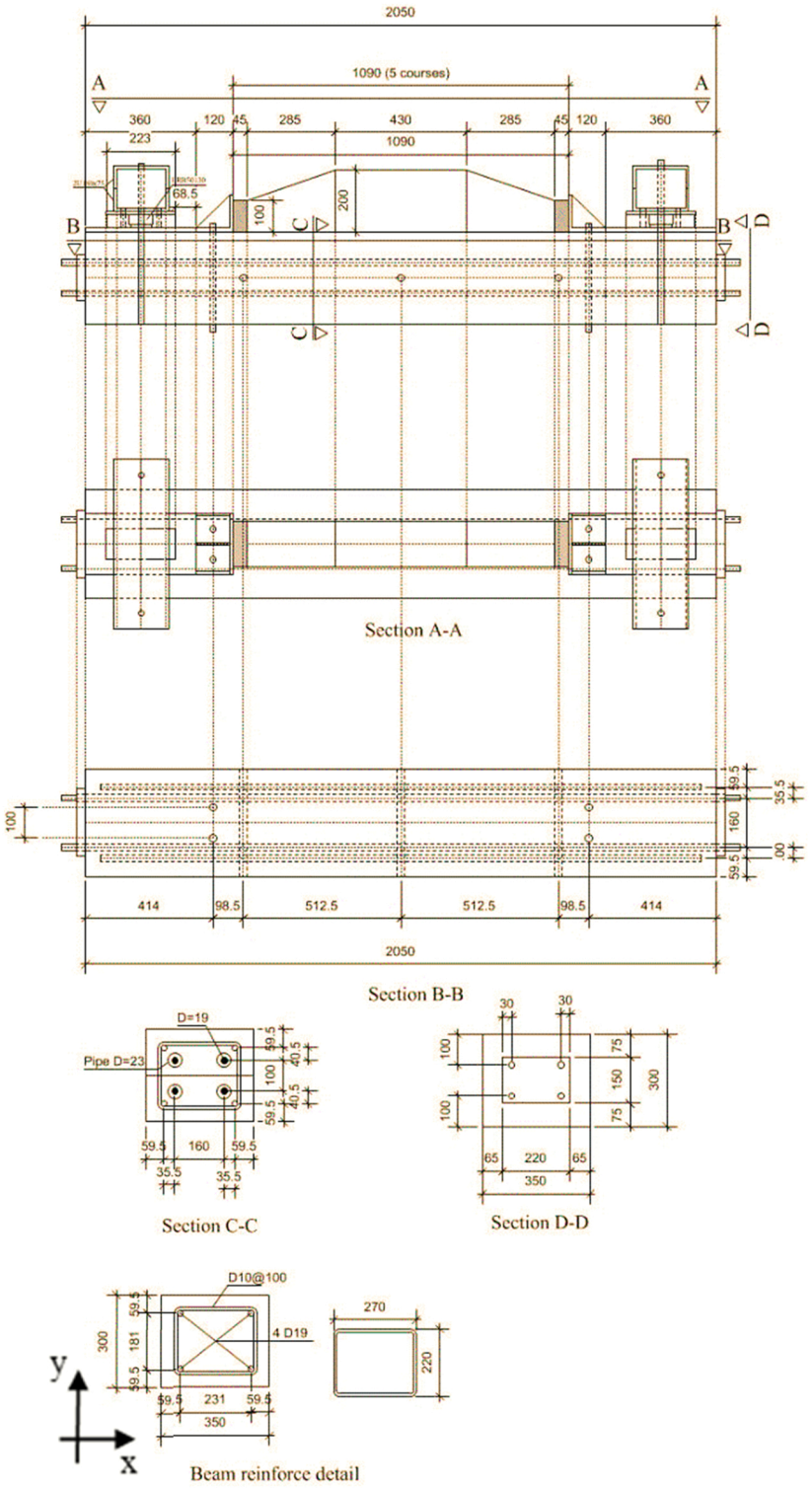

Fig. 8. Detailes of connection of specimen to upper beam.

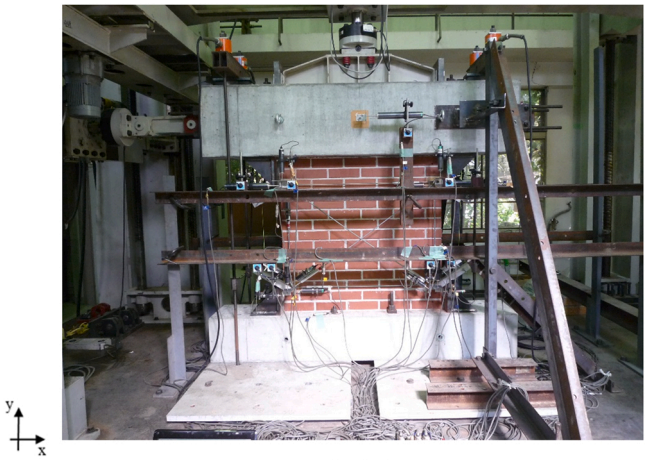

Fig. 9. Pictures of test setup.

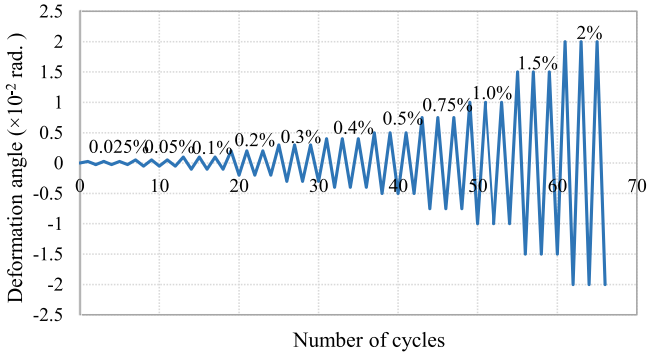

Fig. 10. Lateral loading protocol.

specimens three times in a row. The deformation angle (drift ratio) was calculated as the ratio of the horizontal relative displacement of the specimen's top beam and the wall height.

3. Test results

The cyclic behavior of the masonry specimens was achieved and investigated according to their failure mode and the lateral load-deformation behavior (hysteresis curves), as shown in Figs. 11 and 12, respectively.

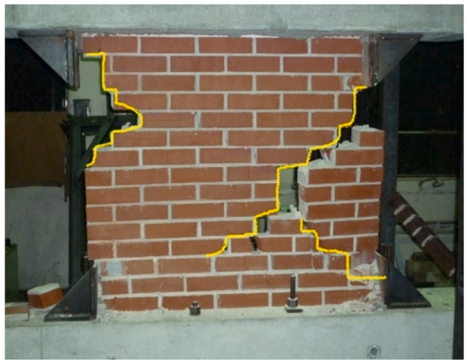

a)

b)

c)

Fig. 11. Failure mode of specimens a) URM b) AFRP-F c) AFRP-X.

3.1. URM specimen

The deformation angle in hysteresis curves was obtained from the ratio of lateral displacement of specimens to their height. The hysteresis curve of the URM specimen shown in Fig. 12(a) demonstrates that the in-plane response of the specimen was linear up until a lateral force of 124 kN and a deformation angle of 0.45×10^{-2} rad. Then, the nonlinear response was initiated by the cracking of the specimen. The horizontal cracks were followed by the diagonal cracks resulting in the stiffness degradation and failure of the URM specimen. Investigation of the hysteresis curve showed that the load-carrying capacity of the URM specimen was 176 kN which was progressively decreased by the propagation and merging of cracks.

3.2. Failure of URM specimen

After the application of cyclic loading on the reference bare wall, it was observed that the failure of the URM specimen was initiated by diagonal cracking with a stepped pattern which was caused by the loss of bond strength between brick and mortar. The propagation and merging of the cracks eventually led to a shear failure of the wall, as shown in Fig. 11(a). This failure mode has been planned to happen in the tests as the most brittle failure state and mainly occurs in the masonry walls with small aspect ratios or lower extent of

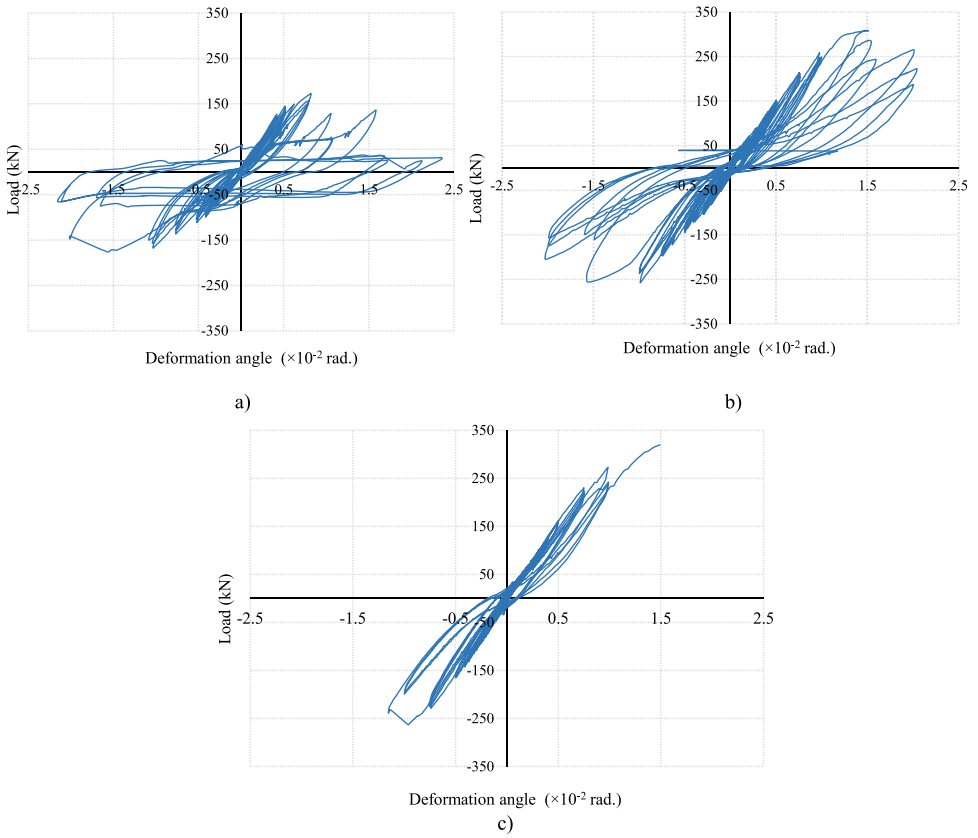

Fig. 12. Hysteresis curve of specimens. a) URM b) AFRP-F c) AFRP-X.

vertical surcharge loads. In shear failure mode, the applied lateral load causes the loss of bond between brick and mortar instead of sliding of brick layers or splitting them.

3.3. Retrofitted specimens (AFRP-F and AFRP-X)

The load-carrying capacity of the AFRP-F and AFRP-X specimens was obtained as 308.67 and 319.42 kN, respectively. In the AFRP-X test, the load value recorded by the loadcell in the final cycle dropped suddenly from 319.42 kN to − 1.01 kN without the usual gradual loss of load value in loading cycles so the data after that point (load drop point) was excluded from the hysteresis curve. Due to larger hysteresis curve loops, the AFRP-F exhibits more energy dissipation capability which is mainly associated with its higher deformability.

3.4. Failure of retrofitted specimen

The failure mode of Fig. 11(b) and (c) demonstrate that, in the retrofitted specimens, the integrity of the specimen was preserved during the experiment and the maximum lateral resistance improved considerably in higher displacements. As shown in Fig. 11(b), while no damage in the AFRP sheet was observed in the AFRP-F specimen, in the AFRP-X specimen, the AFRP sheet ruptured presented in Fig. 11(c). Unlike the reference bare specimen, simultaneous formation of cracks in brick and mortar was detected in the retrofitted specimens, which led to the crushing of the wall toe and tearing of the AFRP sheet in AFRP-F and AFRP-X specimens, respectively.

Table 3
Maximum yield strength and corresponding deformation angle.

Specimen	*URM*	*AFRP-F*	*AFRP-X*
Maximum yield strength (kN)	*176*	*308.67*	*319.42*
ratio to URM specimen	*(1)*	*(1.75)*	*(1.81)*
Deformation angle at maximum load capacity (×10^{-2} rad.)	*1.57*	*1.49*	*1.49*

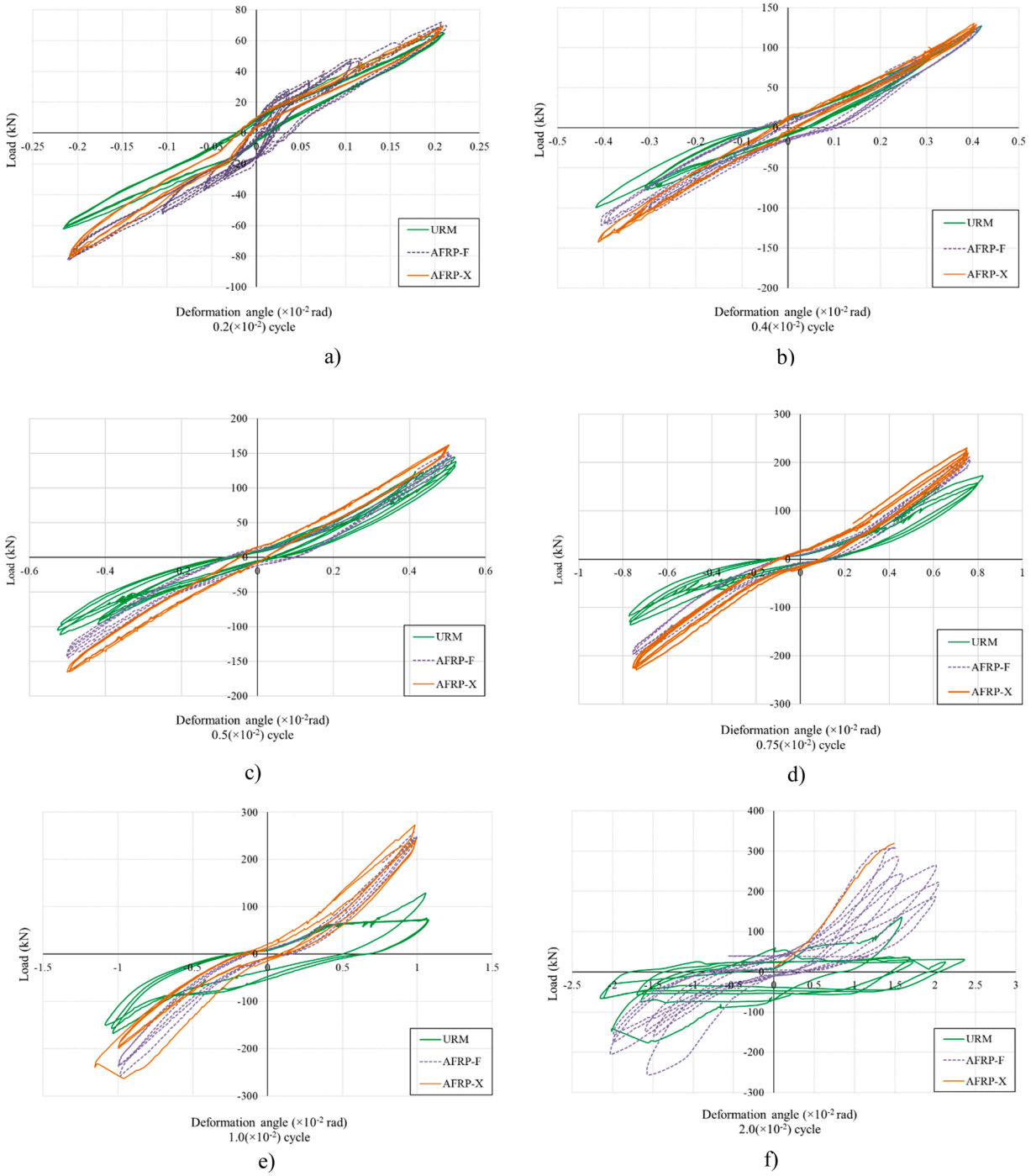

Fig. 13. Hysteresis curves of specimens in different deformation angles.

3.5. Discussion

The maximum yield strength and corresponding deformation angle of each specimen are shown in Table 3 which is taken out from the hysteresis curves of Fig. 13. The maximum yield strength of the wall is defined as the highest load-bearing capacity in the loading cycles. Comparing the values reveals a considerable increase in the retrofitted specimens compared to the bare ones. The shear strength of the retrofitted specimens was increased by 75.4% and 81.5% for the fully-wrapped and the diagonally-wrapped specimens, respectively. Also, an identical amount of the deformation angle corresponding to maximum load capacity was obtained for both

Table 4
Maximum yield strength of specimens in loading cycles.

Cycles	*Maximum yield strength of different deformation angles (kN)*		
	URM	*AFRP-F*	*AFRP-X*
0.1 × 10^{-2}rad.	*41.3*	*44.2*	*34.5*
0.2 × 10^{-2}rad.	*64.61*	*72.03*	*69.52*
0.4 × 10^{-2}rad.	*126.12*	*126.01*	*128.05*
0.5 × 10^{-2}rad.	*142.49*	*152.2*	*162.19*
0.75 × 10^{-2}rad.	*168.51*	*208.72*	*223.91*
1.0 × 10^{-2}rad.	*122.19*	*255.29*	*268.74*
1.5 × 10^{-2}rad.	*117.52*	*308.67*	*319.42*

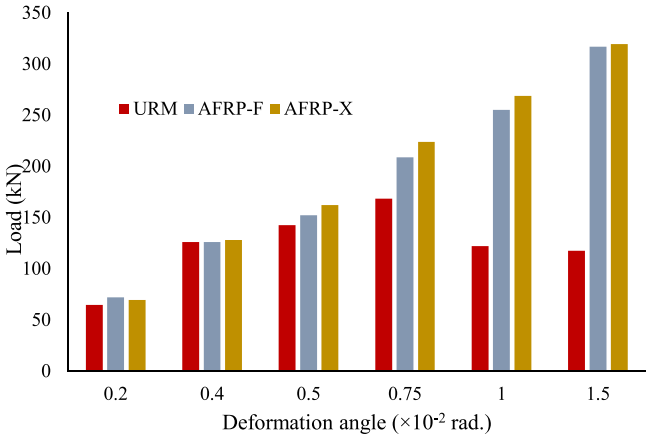

Fig. 14. Comparison of shear strength of specimens in successive loading cycles.

AFRP-F and AFRP-X specimens as 1.49 × 10^{-2} rad. However, the masonry wall units (bricks) tend to behave like separate parts even in smaller displacements, and, the bigger deformation angle of the unreinforced wall at maximum load capacity (1.57 ×10^{-2} rad.) cannot be interpreted as to its deformability. Moreover, the maximum deformation angle provided by the URM specimen before its failure is 2.34 × 10^{-2} rad., while for AFRP-F and AFRP-X specimens, were obtained as 2.04 × 10^{-2} rad. and 1.49 × 10^{-2} rad., respectively. It shows that the fully-wrapped specimen exhibited a deformation capability of about 37% higher than the diagonally-wrapped one. Furthermore, according to Fig. 8, the larger hysteresis curve loops of the two retrofitted specimens represent higher energy dissipation capability.

The hysteresis curves of the specimens are illustrated in Fig. 9 for different deformation angles of 0.2, 0.4, 0.5, 0.75, 1.0, and 2.0 (×10^{-2}) rad. Also, the maximum load-carrying capacity in different deformation angles is presented in Table 4 for each specimen during the successive loading cycles and compared in Fig. 14. According to the hysteresis curves, the maximum load-carrying capacity of the specimens is reduced during consecutive loading cycles. While, in initial sequential cycles (0.1 ×10^{-2}-0.5 ×10^{-2} rad.), the bare and retrofitted specimens exhibit almost an identical lateral stiffness, the stiffness of the URM specimen decreases drastically from the middle cycles (0.5 ×10^{-2} rad.), and the wall undergoes a considerable loss of shear strength. Also, as shown in Fig. 13(a-c), the shear load-carrying behavior of the three specimens in initial cycles is almost the same, and no significant load-carrying capacity was added to the specimen due to retrofitting. According to Fig. 13(d), when the retrofitted wall reaches the maximum bearable force of URM, the additional load is transferred to the AFRP sheet. Unlike the bare reference specimen, the stiffness reduction does not occur drastically in the retrofitted specimens. In the latter half of the loading cycles, shown in Fig. 13(d-f), where the URM specimen completely loses its stiffness, almost the same load-carrying capacity for the two retrofitted specimens was observed.

It reveals that the maximum yield strength of the sequential cyclic deformation angles for both AFRP-F and AFRP-X specimens exhibit a similar decreasing trend with almost identical data. In the first stages of cyclic loading, due to the confining effect of the AFRP layer, only the compressive behavior of the specimen is improved by retrofitting while the tensile behavior of both URM and retrofitted specimens is almost the same. In larger deformation angles, by the propagation of cracks, the masonry loses its tensile load-carrying capacity and the retrofit layer contributes to the tensile behavior as well as the compressive one. However, due to the different load transfer mechanisms of the two retrofit configurations, the contribution of the AFRP layer to the deformation capacity of the retrofitted specimens is different. AFRP-X withstands the transferred load by a bracing action which increases the tensile stress in diagonal strips and eventually leads to their rupture. The stress in AFRP-F is distributed by in-plane shear and bending actions which cannot reach the rupture point. So the wall specimen keeps its integrity and starts rocking as a whole body. While this action provides additional deformation capacity for the specimen, it increases the compressive stress at the wall toe and eventually causes compressive crushing there.

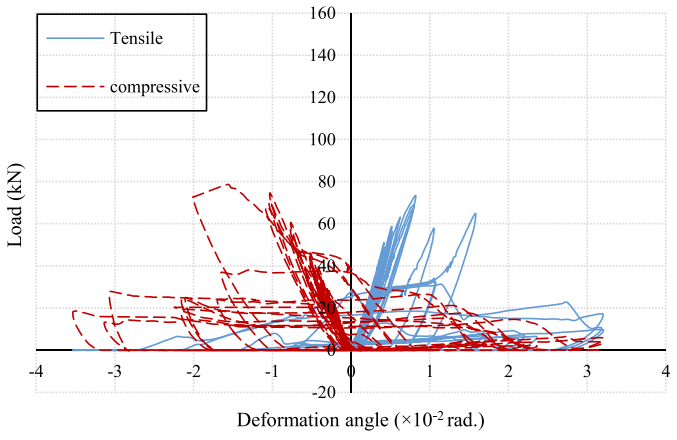

a)

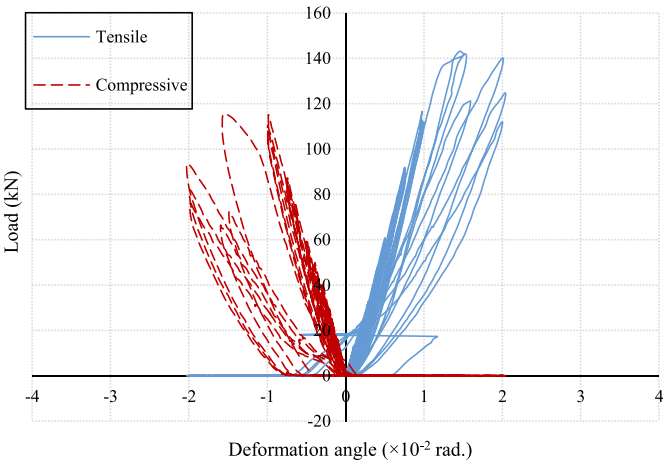

b)

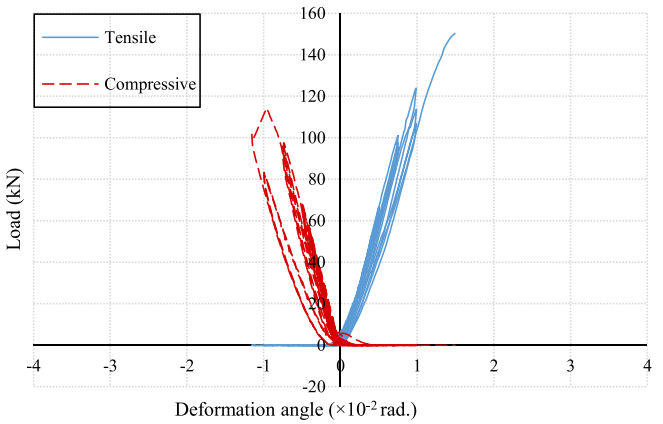

c)

Fig. 15. Load-deformation angle diagram of specimens. a) URM b) AFRP-F c) AFRP-X.

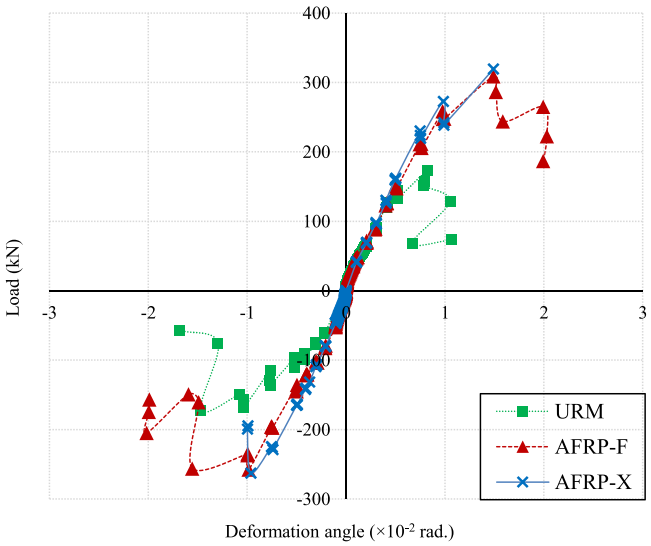

Fig. 16. Backbone curves of specimens.

The tensile and compressive behavior of the specimens during cyclic loading are compared in Fig. 15, in which, all load data of the tension and compression half-cycles were transferred to the positive side of the load axes in the hysteresis curve. While the URM specimen did not behave similarly in the half-cycles of loading, the higher degree of symmetry in the hysteresis curves represents a more consistent behavior and integrity in the retrofitted specimens.

The backbone curves (load-deformation envelopes) of the specimens are shown in Fig. 16. The maximum deformation angle of 2×10^{-2} rad. for the fully-wrapped specimen compared to the one of the diagonally-wrapped specimen (1.5×10^{-2} rad.), reveals that the AFRP-F specimen exhibits higher ultimate deformation capability than AFRP-X. In addition, the URM and retrofitted wall specimens demonstrated an identical initial stiffness which means that AFRP retrofitting did not alter the stiffness of the masonry wall.

In the current study, the hysteresis behavior of the specimens was obtained experimentally which can be obtained alternatively by employing numerical methods. There are novel and strong numerical methods that have been recently proposed to establish and solve the load-displacement curve of anisotropic media. Among them, the "Galerkin" [40] and "Bezier" [41] methods have proven to provide higher stability and accuracy than other numerical methods (including FEM).

4. Conclusion

In this paper, the results of an experimental study on the cyclic in-plane behavior of the AFRP retrofitted masonry walls were reported and discussed. A cyclic lateral load along with vertical load were applied to the URM reference specimen and the other two specimens retrofitted in fully-covered and diagonally-wrapped configurations. The effect of AFRP retrofitting was evaluated in terms of hysteresis behavior and failure mode.

The obtained results of the study are summarized as follows:

1. The shear strength of the AFRP retrofitted masonry wall increased by 75.4% and 81.5% for the fully-wrapped and the diagonally-wrapped specimens, respectively.
2. While the shear capacity of the diagonally-wrapped retrofitted masonry wall was obtained slightly higher than the fully-wrapped one – with an identical corresponding deformation angle -, the fully-wrapped specimen exhibits higher ultimate deformation capability than the diagonally-wrapped specimen.
3. Although the URM wall specimen did not behave similarly in tension and compression half-cycles of loading, the symmetry in the hysteresis curve represents a more consistent and integrated lateral behavior in the retrofitted specimens.
4. According to the failure modes of the retrofitted specimens, the failure of the fully-wrapped specimen was controlled by toe crushing of masonry, while the tearing of the AFRP sheet caused the failure in the diagonally-wrapped specimen.
5. Hysteresis curves of the URM and retrofitted wall specimens demonstrate an identical initial stiffness. In other words, AFRP retrofitting did not alter the lateral stiffness of the masonry wall.

In order to have a better evaluation of the effectiveness of AFRP retrofitting on the cyclic behavior of URM walls, the load-carrying and deformation capacity of the specimens should be compared to other retrofitting methods which was not carried out in this study. The effect of AFRP on the out-of-plane behavior of the URM wall should also be studied. Moreover, the impact of different configurations of AFRP retrofitting with different fiber reinforcement ratios should be compared.

The study results showed that AFRP as a soft product of FRP materials has a considerable capability for enhancing the cyclic

behavior of URM walls which are best known for their weak in-plane response. Therefore, AFRP could be a promising future for seismic retrofitting of masonry structures. Further research is required to identify and evaluate the feasibility of this retrofit technique.

Declaration of Competing Interest

The authors declare that they have no known competing financial interests or personal relationships that could have appeared to influence the work reported in this paper.

Data availability

Data will be made available on request.

References

[1] H. Matthys, L. Noland, Evaluation, Strengthening, and Retrofitting of Masonry Buildings, TMS, Colorado, 1989.
[2] D.P. Abrams, Performance-based engineering concepts for unreinforced masonry building structures, Prog. Struct. Eng. Mater. 3 (1) (2001) 48–56.
[3] M. ElGawady, P. Lestuzzi, M. Badoux, A review of conventional seismic retrofitting techniques for URM, in: Proceedings of the 13th International Brick and Block Masonry Conference, 2004, pp. 1–10.
[4] A.M. Halabian, L. Mirshahzadeh, H. Hashemol-Hosseini, Non-linear behavior of unreinforced masonry walls with different Iranian traditional brick-work settings, Eng. Fail. Anal. 44 (2014) 46–65.
[5] N. Gattesco, I. Boem, Out-of-plane behavior of reinforced masonry walls: experimental and numerical study, Compos. Part B Eng. 128 (2017) 39–52.
[6] T. Bakeer, Assessment the stability of masonry walls by the transfer-matrix method, Eng. Struct. 110 (2016) 1–20.
[7] ASCE, ASCE/SEI 41-17, Seismic Evaluation and Retrofit of Existing Buildings, American Society of Civil Engineers, Reston, VA, USA, 2017.
[8] H.A. Khan, R.P. Nanda, D. Das, In-plane strength of masonry panel strengthened with geosynthetic, Constr. Build. Mater. 156 (2017) 351–361.
[9] G.Z. Ahari, K. Yamaguchi, A proposal of the most suitable retrofitting methods for URM structures in Iran. An extensive review of recent techniques, J. Habitat Eng. 2 (2) (2010) 105–114.
[10] Z. Al-Jabari, J.J. Myers, M. ElGawady, Effectiveness of FRCM system in strengthening reinforced masonry walls subjected to cyclic loading, in: IABSE Symposium Report, International Association for Bridge and Structural Engineering, 109(39), 2017.
[11] E. Vintzileou, E. Panagiotidou, An empirical model for predicting the mechanical properties of FRP-confined concrete, Constr. Build. Mater. 22 (5) (2008) 841–854.
[12] Y. Zhuge, FRP-retrofitted URM walls under in-plane shear: review and assessment of available models, J. Compos. Constr. 14 (6) (2010) 743–753.
[13] M.R. Ehsani, H. Saadatmanesh, A. Al-Saidy, Shear behavior of URM retrofitted with FRP overlays, J. Compos. Constr. 1 (1) (1997) 17–25.
[14] M.A. ElGawady, P. Lestuzzi, M. Badoux, Aseismic retrofitting of unreinforced masonry walls using FRP, Compos. Part B Eng. 37 (2–3) (2005) 148–162.
[15] M.A. ElGawady, P. Lestuzzi, M. Badoux, Shear strength of URM walls retrofitted using FRP, Eng. Struct. 28 (12) (2006) 1658–1670.
[16] A. Jafari, A.V. Oskouei, M. Bazli, R. Ghahri, Effect of the FRP sheet's arrays and NSM FRP bars on in-plane behavior of URM walls, J. Build. Eng. 20 (2018) 679–695.
[17] K.M.C. Konthesingha, M.J. Masia, R.B. Petersen, N. Mojsilovic, G. Simundic, A.W. Page, Static cyclic in-plane shear response of damaged masonry walls retrofitted with NSM FRP strips–an experimental evaluation, Eng. Struct. 50 (2013) 126–136.
[18] D. Zhou, Z. Lei, J. Wang, In-plane behavior of seismically damaged masonry walls repaired with external BFRP, Compos. Struct. 102 (2013) 9–19.
[19] Z.A. Al-Jaberi, J.J. Myers, M.A. ElGawady, Evaluation of FRP and FRCM composites for the strengthening of reinforced masonry walls, J. Am. Concr. Inst. 327 (2018), 32-1.
[20] Z.K. Aljaberi, J.J. Myers, M.E. ElGawady, A comparative study of flexural behavior of reinforced masonry walls strengthened with near-surface mounted FRP bars or externally bonded FRP sheets. Insights and Innovations in Structural Engineering, Mechanics and Computation, CRC Press, 2016, pp. 1459–1464.
[21] P. Roca, G. Araiza, Shear response of brick masonry small assemblages strengthened with bonded FRP laminates for in-plane reinforcement, Constr. Build. Mater. 24 (8) (2010) 1372–1384.
[22] G. Zamani Ahari, K. Yamaguchi, H. Tanaka, Shear behavior of masonry specimens strengthened with aramid fiber reinforced polymer sheet, J. Archit. Urban Des. 23 (2013) 47–53.
[23] M. Kaliraj, P. Narayanasamy, M. Rajkumar, M.M. Mohaideen, I.N. Manickam, Design, fabrication and analysis of advanced polymer based kevlar-49 composite material, Appl. Mech. Mater. 592 (2014) 122–127.
[24] K. Brózda, J. Selejdak, P. Koteš, The analysis of beam reinforced with FRP bars in bending, Procedia Eng. 192 (2017) 64–68.
[25] X. Kong, X. Qi, Y. Gu, I.A. Lawan, Y. Qu, Numerical evaluation of blast resistance of RC slab strengthened with AFRP, Constr. Build. Mater. 178 (2018) 244–253.
[26] M. Menegotto, G. Monti, S. Salvini, M. Vailati, Improvement of transverse connection of masonry walls through afrp bars. Advances in FRP Composites in Civil Engineering, Springer, Berlin, Heidelberg, 2011, pp. 947–950.
[27] A. Dutu, H. Sakata, Y. Yamazaki, T. Shindo, Retrofit solution for timber framed masonry system using aramid fiber reinforced polymers (AFRP), in: IABSE Conference: Elegance in structures, Nara, Japan, 13–15 May 2015, pp. 210–211.
[28] E. Pinotti, C. Casalegno, R. Ceravolo, C. Surace, Aramid fibres for conservative intervention on masonry structures, in: Brick and Block Masonry: Proceedings of the 16th International Brick and Block Masonry Conference, Padova, Italy, CRC Press, 26–30 June 2016, pp. 2153–2160.
[29] M. Vailati, G. Monti, Strengthening of masonry walls by transverse connection through AFRP rods: experimental tests and analytical models, NED Univ. J. Res., 2012.
[30] H.J. Kim, T.W. Park, S.H. Cho, K.K. Lee, Y.S. Roh, L. Chung, Experimental study on seismic retrofitting methods for school building using aramid strip, J. Korean Soc. Saf. 25 (3) (2010) 100–106.
[31] D. Zhu, B. Mobasher, A. Vaidya, S.D. Rajan, Mechanical behaviors of Kevlar 49 fabric subjected to uniaxial, biaxial tension and in-plane large shear deformation, Compos. Sci. Technol. 74 (2013) 121–130.
[32] ASTM C67/C67M-20, Standard Test Methods for Sampling and Testing Brick and Structural Clay Tile, 2020.
[33] G.Z. Ahari, K. Yamaguchi, H. Nishiyama, M. Miyajima, An experimental study on the retrofitting of unreinforced masonry specimens with ECC and AFRP sheet, J. Struct. Eng. 59B (2013) 81–91.
[34] C. ASTM, Standard Test Method for Compressive Strength of Masonry Prisms, Masonry Test Methods and Specifications for the Building Industry, 2012.
[35] C. ASTM, Standard Test Method for Flow of Hydraulic Cement Mortar, C1437, 2007.
[36] ASTM C138/C138M-17a, Standard Test Method for Density (Unit Weight), Yield, and Air Content (Gravimetric) of Concrete, 2017.
[37] ASTM International Committee C09 on Concrete and Concrete Aggregates, Standard Test Method for Static Modulus of Elasticity and Poisson's Ratio of Concrete in Compression1, ASTM International, 2014.
[38] A.S.T.M. Standard, Standard Test Method for Compressive Strength of Cylindrical Concrete Specimens, ASTM C39, 2010.

[39] FEMA, Interim Protocols for Determining Seismic Performance Characteristics of Structural and Nonstructural Components through Laboratory Testing, FEMA 461, 2007.
[40] V.G. Belardi, P. Fanelli, F. Vivio, Bending analysis with Galerkin method of rectilinear orthotropic composite circular plates subject to transversal load, Compos. Part B Eng. 140 (2018) 250–259.
[41] H. Kabir, M.M. Aghdam, A robust Bézier based solution for nonlinear vibration and post-buckling of random checkerboard graphene nano-platelets reinforced composite beams, Compos. Struct. 212 (2019) 184–198.